Int. J. Heat Mass Transfer. Vol. 32, No. 3, pp. 493–501, 1989
Printed in Great Britain

0017–9310/89 $3.00 + 0.00

Leading edge effects on free convection of a Darcian fluid about a semi-infinite vertical plate with uniform heat flux

I. POP
Faculty of Mathematics, University of Cluj, R-3400 Cluj, CP 253, Romania

and

P. CHENG and T. LE
Department of Mechanical Engineering, University of Hawaii at Manoa, Honolulu, HI 96822, U.S.A.

(*Received* 15 *April* 1988 *and in final form* 15 *July* 1988)

Abstract—The method of matched asymptotic expansions, together with a deformed longitudinal coordinate, is applied to study the leading edge effect on free convection about a semi-infinite, uniform heat flux, vertical surface embedded in a porous medium. The leading edge effect manifests itself as inhomogeneous terms in the second- and third-order problems. Similarity solutions for the free convection porous-media flow are obtained up to the third-order approximation. It is shown that the leading edge effect increases the streamwise vertical velocity near the outer edge of the thermal boundary layer, resulting in a corresponding increase in heat flux. The leading edge and the entrainment effects are shown to increase the heat transfer rate almost equally. At $Ra_x = 100$, the combined effects enhance the heat transfer rate by more than 10% as compared with those based on the boundary layer approximation. These effects increase as the Rayleigh number is decreased.

INTRODUCTION

FLOW VISUALIZATION studies [1] of natural convection about a heated vertical plate suggest that the thermal boundary layer does not start at the leading edge of the plate, as usually assumed in the boundary layer approximation. These phenomena have been attributed to the induced flow upstream of the leading edge, generally known as the leading edge effect [1–4]. Using the method of matched asymptotic expansions, Hieber [3] as well as Martynenko *et al.* [4] have shown that the leading edge effects increase surface heat flux as compared to those predicted by the classical boundary layer theory. With the effects of the leading edge and boundary layer entrainment taken into consideration, Martynenko *et al.* [4] found that the predicted velocity profiles and Nusselt numbers are in better agreement with experimental data especially at low Rayleigh numbers.

The akin problem of natural convection about a semi-infinite heated vertical plate embedded in a porous medium has attracted considerable attention during the past decade [5–20]. Most of the Nusselt number data [8–11] are found to be higher than those predicted by Cheng and Minkowycz's similarity solution [5], which is based on Darcy's law with boundary layer approximation invoked. The higher experimentally determined Nusselt numbers have been attributed to the fact that the effects of near-wall porosity variation [15, 16], transverse thermal dispersion [17, 18] and boundary layer entrainment [19, 20] have been neglected in Cheng and Minkowycz's analysis. The purpose of this paper is to point out that the leading edge effect, which has been neglected in Cheng and Minkowycz's theory [5], is also partially responsible for the higher experimental Nusselt numbers.

In this paper, the approach used by Martynenko *et al.* [4] is applied to the problem of natural convection about a semi-infinite, vertical, uniform heat flux surface embedded in a porous medium. The formulation of the problem is based on Darcy's law which is valid when the particle diameter to plate length ratio is small, a condition consistent with the existing experimental data [8–12]. It is shown that the leading edge effect enters the second- and third-order problems as inhomogeneous terms in the equations and boundary conditions. For $Ra_x = 100$, it is found that the leading edge and boundary layer entrainment effects enhance the heat transfer rate by more than 10% over those predicted by Cheng and Minkowycz's similarity solution [5]. These effects increase with decreasing Rayleigh number.

ANALYSIS

The governing equations (in terms of dimensionless stream function ψ and temperature θ) for natural convection in a porous medium, adjacent to a vertical

NOMENCLATURE

a constant in equation (69)
a_0 constant defined in equation (45)
a_1 constant defined in equation (41a)
a_n constant defined in equation (41b)
A_1 constant defined in equation (38)
b constant defined in equation (69)
c constant defined in equation (69)
C_1 constant defined in equation (66)
F function defined in equation (8c)
f_0, f_1, f_2 first-, second- and third-order inner stream functions
g gravitational acceleration
g_0, g_1, g_2 first-, second- and third-order inner temperature functions
k thermal conductivity of the saturated porous medium
K permeability of the porous medium
l length of the plate
L function defined in equation (67)
n exponent in equation (39)
Nu_x local Nusselt number, $q_w\hat{x}/k(T_w-T_\infty)$
$(Nu_x)_{B.L.}$ local Nusselt number based on boundary layer theory
q_w surface heat flux
r radius of the polar coordinates
Ra Rayleigh number of the porous medium based on l, $g\beta Kq_w l^2/\alpha\nu k$
Ra_x Rayleigh number of the porous medium based on x, $g\beta Kq_w\hat{x}^2/\alpha\nu k$
T dimensional temperature
$\hat{u}, u$ dimensional and dimensionless vertical velocities
$\hat{v}, v$ dimensional and dimensionless horizontal velocities
$\hat{x}, x$ dimensional and dimensionless vertical coordinates, $x = \hat{x}/l$
X dimensionless deformed longitudinal coordinate defined in equation (8c)
X_0 distance between the origin of the thermal boundary layer and the leading edge
$\hat{y}, y$ dimensional and dimensionless horizontal coordinates, $y = \hat{y}/l$
Y dimensionless inner variable defined in equation (8b).

Greek symbols

α thermal diffusivity of the porous medium
α_m eigenvalues
β coefficient of thermal expansion of fluid
ε perturbation parameter based on l, $Ra^{-1/3}$
ε_x perturbation parameter based on x, $Ra_x^{-1/3}$
η similarity variable defined in equation (19c)
θ dimensionless temperature, $k(T-T_\infty)/q_w l$
$\Theta_0, \Theta_1, \Theta_2$ first-, second- and third-order inner perturbation solutions for temperature
Λ angle of the polar coordinate
ν kinematic viscosity of the fluid
$\hat{\psi}, \psi$ dimensional and dimensionless stream functions, $\psi = k\nu\hat{\psi}/g\beta Kq_w l^2$
ψ_0, ψ_1, ψ_2 first-, second- and third-order outer perturbation stream function
$\tilde{\psi}_1$ perturbation function defined in equation (51)
Ψ dimensionless inner stream function
Ψ_0, Ψ_1, Ψ_2 first-, second- and third-order inner perturbation stream function.

plate with uniform heat flux, based on Darcy's law and Boussinesq approximation are

$$\psi_{xx}+\psi_{yy} = \theta_y \tag{1}$$

$$\varepsilon^3(\theta_{xx}+\theta_{yy}) = \psi_y\theta_x-\psi_x\theta_y. \tag{2}$$

In the above equations, the dimensionless variables are defined as

$$x = \hat{x}/l, \qquad y = \hat{y}/l,$$

$$\psi = k\nu\hat{\psi}/g\beta Kq_w l^2, \quad \theta = k(T-T_\infty)/q_w l \tag{3}$$

with

$$u = \frac{\hat{u}}{\hat{u}_r} = \psi_y, \quad v = \frac{\hat{v}}{\hat{u}_r} = -\psi_x, \quad \hat{u}_r = \frac{g\beta q_w Kl}{k\nu}$$

where l is a reference length; $\hat{x}$ and $\hat{y}$ the vertical and horizontal coordinates with the origin placed on the leading edge of the plate; $\hat{u}$ and $\hat{v}$ the Darcian velocities in the $\hat{x}$- and $\hat{y}$-directions; ν and β the kinematic viscosity and thermal expansion coefficient of the fluid; K the permeability of the porous medium; q_w the prescribed surface heat flux; k the thermal conductivity of the saturated porous medium; T the temperature; and g the gravitational acceleration. The quantity ε in equation (2) is defined as $\varepsilon = Ra^{-1/3}$ where $Ra = g\beta Kq_w l^2/\alpha\nu k$ is the modified Rayleigh number based on the reference length l. The dimensionless boundary conditions are given by

$$y = 0, \quad x > 0: \quad \psi_x = 0, \quad \theta_y = -1 \tag{4a, b}$$

$$y = 0, \quad x < 0: \quad \psi_x = 0, \quad \theta_y = 0 \tag{5a, b}$$

$$r \to \infty, \quad \Lambda = \tan^{-1}\left(\frac{y}{x}\right) \neq 0, \quad \psi_y = 0, \quad \theta = 0 \tag{6a, b}$$

where (r, Λ) are the polar coordinates.

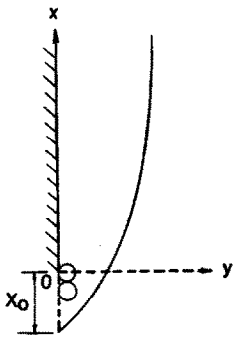

FIG. 1. Coordinate system

We now attempt to solve equations (1) and (2) subject to boundary conditions (4)–(6) under the condition $\varepsilon \to 0$ by means of the method of matched asymptotic expansions with a deformed longitudinal coordinate. To this end, the dependent variables of the inner problem will be expanded as

$$\Psi(x,y;\varepsilon) = \varepsilon^2[\Psi_0(X,Y)+\varepsilon\Psi_1(X,Y)+\varepsilon^2\Psi_2(X,Y) + \varepsilon^{\alpha_m}\Psi_m(X,Y)+\text{h.o.t.}] \quad (7a)$$

and

$$\theta(x,y;\varepsilon) = \varepsilon[\Theta_0(X,Y)+\varepsilon\Theta_1(X,Y)+\varepsilon^2\Theta_2(X,Y) + \varepsilon^{\alpha_m}\Theta_m(X,Y)+\text{h.o.t.}] \quad (7b)$$

with

$$\psi = \Psi, \quad y = \varepsilon Y \quad (8a,b)$$

and

$$x = X+\varepsilon F(X,Y)+\ldots \quad (8c)$$

where the longitudinal coordinate x is deformed so that the real position of the boundary layer relative to the leading edge of the surface can be determined (Fig. 1). The function $F(X,Y)$ in equation (8c) will be determined later from the condition of the similarity solution in the boundary layer, and the exponential decays of the second-order longitudinal velocity at the outer edge of the boundary layer. From equations (8) we obtain the following transformations:

$$\frac{\partial}{\partial x} = \frac{\partial}{\partial X} - \varepsilon F_X\frac{\partial}{\partial X} + \varepsilon^2 F_X^2\frac{\partial}{\partial X} + \text{h.o.t.} \quad (9a)$$

$$\frac{\partial}{\partial y} = \varepsilon^{-1}\frac{\partial}{\partial Y} - F_Y\frac{\partial}{\partial X} + \varepsilon F_X F_Y\frac{\partial}{\partial X} + \text{h.o.t.} \quad (9b)$$

and

$$\frac{\partial^2}{\partial x^2} = \frac{\partial^2}{\partial X^2} - 2\varepsilon F_X\frac{\partial^2}{\partial X^2} - \varepsilon F_{XX}\frac{\partial}{\partial X} + \text{h.o.t.} \quad (10a)$$

$$\frac{\partial^2}{\partial y^2} = \varepsilon^{-2}\frac{\partial^2}{\partial Y^2} - 2\varepsilon^{-1}F_Y\frac{\partial^2}{\partial X\partial Y} + 2F_X F_Y\frac{\partial^2}{\partial X\partial Y} + F_Y^2\frac{\partial^2}{\partial X^2} + \text{h.o.t.} \quad (10b)$$

where

$$F_X = \frac{\partial F}{\partial X}, \quad F_Y = \frac{\partial F}{\partial Y}, \quad \frac{\partial X}{\partial x} = 1-\varepsilon F_X \quad \text{and} \quad \frac{\partial X}{\partial Y} = -F_Y. \quad (10c)$$

With the aid of equations (9) and (10), equations (1) and (2) can be expressed in terms of the inner variables X and Y to give

$$\frac{1}{\varepsilon^2}\psi_{YY} - \frac{2F_Y}{\varepsilon}\psi_{XY} + \psi_{XX} + 2F_X F_Y\psi_{XY} + F_Y^2\psi_{XX} - \varepsilon[2F_X\psi_{XX}+F_{XX}\psi_X] = \frac{1}{\varepsilon}\theta_Y - F_Y\theta_{XX} + \varepsilon F_X F_Y\theta_X \quad (11a)$$

and

$$\theta_{YY} - 2F_Y\theta_{XY} + \varepsilon^2(2F_Y\theta_{XY}+F_Y\theta_{XX}+\theta_{XX}) - \varepsilon^3(2F_X\theta_{XX}+F_{XX}\theta_X) = \frac{1}{\varepsilon}(\psi_Y\theta_X - \psi_X\theta_Y) + F_X(\psi_X\theta_Y - \psi_Y\theta_X) + \varepsilon F_X^2(\psi_Y\theta_X - \psi_X\theta_Y). \quad (11b)$$

For the outer problem, the dependent variables can be expanded as

$$\psi(x,y;\varepsilon) = \varepsilon^2[\psi_0(X,y)+\varepsilon\psi_1(X,y)+\text{h.o.t.}] \quad (12a)$$

$$\theta(x,y;\varepsilon) = 0 \quad (12b)$$

where X is the deformed coordinate given by equation (8c). With the aid of equations (12b) and (10a), equation (1) in terms of the outer variables X and y is given as

$$\psi_{XX}+\psi_{yy}-2\varepsilon F_X\psi_{XX}-\varepsilon F_{XX}\psi_X = 0. \quad (13)$$

The matching conditions are given by

$$\psi_y(X,0) = \Psi_y(X,\infty), \quad \psi_{yy}(X,0) = \Psi_{yy}(X,\infty). \quad (14a,b)$$

With the aid of equations (7a) and (12a) and transformations (9b) and (10b), the above matching conditions can be written as

$$\varepsilon^2\psi_{0y}(X,0)+\varepsilon^3\psi_{1y}(X,0) = \varepsilon\Psi_{0Y}(X,\infty) + \varepsilon^2(\Psi_{1Y}-F_Y\Psi_{0X})_{X,\infty} + \varepsilon^3(\Psi_{2Y}-F_Y\Psi_{1X} + F_X F_Y\Psi_{0X})_{X,\infty}+\text{h.o.t.} \quad (15a)$$

and

$$\varepsilon^2\psi_{0yy}(X,0) = \Psi_{0YY}(X,\infty)+\varepsilon(\Psi_{1YY}-2F_Y\Psi_{0X,Y})_{X,\infty} + \varepsilon^2(\Psi_{2YY}-2F_Y\Psi_{1XY}+2F_X F_Y\Psi_{0XY}+F_Y^2\Psi_{0XX})_{X,\infty}. \quad (15b)$$

First-order inner problem

Substituting equation (7) into equation (11) leads to the following first-order inner problem:

$$\Psi_{0YY} = \Theta_{0Y} \quad (16a)$$

$$\Theta_{0YY} = \Psi_{0Y}\Theta_0 - \Psi_{0X}\Theta_{0Y} \tag{16b}$$

subject to the boundary conditions

$$Y = 0: \quad \Psi_{0X} = 0, \quad \Theta_{0Y} = -1 \tag{17a, b}$$

and

$$Y \to \infty: \quad \Psi_{0Y} = 0, \quad \Theta_0 = 0. \tag{18a, b}$$

Equations (16)–(18) show that the effect of the deformed longitudinal coordinate does not enter the first-order inner problem. Equations (16)–(18) admit a similarity solution of the form [5, 6]

$$\Psi_0 = X^{2/3} f_0(\eta), \quad \Theta_0 = X^{1/3} g_0(\eta), \quad \eta = Y/X^{1/3} \tag{19a–c}$$

where $f_0(\eta)$ and $g_0(\eta)$ satisfy the following equations:

$$f_0''' = g_0' \tag{20}$$

$$g_0'' + \tfrac{2}{3} f_0 g_0' - \tfrac{1}{3} f_0' g_0 = 0 \tag{21}$$

with boundary conditions

$$f_0(0) = g_0'(0) + 1 = 0 \tag{22a, b}$$

$$f_0'(\infty) = g_0(\infty) = 0 \tag{23a, b}$$

where the primes denote differentiation with respect to η. It follows from equation (19a) that

$$\Psi_0(X, \infty) = X^{2/3} f_0(\infty). \tag{24}$$

First-order outer problem

Substituting equation (12a) into equation (13) yields the following first-order outer problem

$$\nabla^2 \psi_0 = 0 \tag{25}$$

with the boundary condition

$$\psi_0(X, 0) = 0, \quad X < 0 \tag{26a}$$

and the matching condition

$$\psi_0(X, 0) = X^{2/3} f_0(\infty), \quad X > 0. \tag{26b}$$

The solution to equations (25) and (26) is [19]

$$\psi_0(X, y) = f_0(\infty) r^{2/3} \sin[\tfrac{2}{3}(\pi - \Lambda)] / \sin\left(\frac{2\pi}{3}\right). \tag{27a}$$

It follows from equation (27a) that

$$\psi_0(X, 0) = f_0(\infty) X^{2/3} \left[1 - \frac{2y}{3X} \cot\left(\frac{2\pi}{3}\right) + \frac{y^2}{9X^2} + \text{h.o.t.}\right]. \tag{27b}$$

Second-order inner problem

Substituting equation (7) into equation (11) leads to the following second-order inner problem:

$$\Psi_{1YY} - \Theta_{1Y} = F_Y(2\Psi_{0XY} - \Theta_{0X}) \tag{28}$$

and

$$\Theta_{1YY} - (\Psi_{0Y}\Theta_{1X} - \Psi_{0X}\Theta_{1Y}) - (\Psi_{1Y}\Theta_{0X} - \Psi_{1X}\Theta_{0Y}) = 2F_Y\Theta_{0XY} + F_X(\Psi_{0X}\Theta_{0Y} - \Psi_{0Y}\Theta_{0X}) \tag{29}$$

with boundary conditions

$$\Psi_{1X}(X, 0) = 0, \quad \Theta_{1Y}(X, 0) = 0 \tag{30a, b}$$

and matching conditions

$$\Psi_{1Y}(X, \infty) - F_Y(X, \infty)\Psi_{0X}(X, \infty) = \psi_{0y}(X, 0) \tag{31a}$$

$$\Theta_1(X, \infty) = 0. \tag{31b}$$

Equations (28)–(31) show that the effect of the deformed longitudinal coordinate enters the second-order inner problem as inhomogeneous terms. It can be shown that equations (28)–(31) admit a similarity solution of the form

$$\Psi_1(X, Y) = f_1(\eta) + F\Psi_{0X} \tag{32}$$

$$\Theta_1(X, Y) = X^{-1/3} g_1(\eta) + F\theta_{0X}. \tag{33}$$

It is relevant to note that the first term on the right-hand side of equation (32) or equation (33) is the homogeneous solution to equations (28)–(31), where $f_1(\eta)$ and $g_1(\eta)$ are determined from [20]

$$f_1''' = g_1' \tag{34}$$

and

$$g_1'' + \tfrac{2}{3} f_0 g_1' + \tfrac{1}{3} f_0' g_1 = \tfrac{1}{3} g_0 f_1' \tag{35}$$

with boundary and matching conditions given by

$$f_1(0) = g_1'(0) = 0 \tag{36a, b}$$

$$g_1(\infty) = 0 \tag{37a}$$

and

$$f_1'(\infty) = -\tfrac{2}{3} f_0(\infty) \cot\left(\frac{2\pi}{3}\right). \tag{37b}$$

It follows from equation (37b) that

$$f_1(\eta) = -\tfrac{2}{3} f_0(\infty)\eta \cot\left(\frac{2\pi}{3}\right) + A_1 + \text{exp}, \quad \text{as } \eta \to \infty. \tag{38}$$

The above equation can be used to determine the constant A_1 after $f_1(\eta)$ is obtained numerically from equations (34)–(37).

We now determine the function $F(X, Y)$ following the procedures given by Martynenko *et al.* [4]. In order that the similarity condition exists in equations (32) and (33), it is required that the function $F(X, Y)$ be of the form

$$F(X, Y) = X^{1/3} \sum_{n=0}^{\infty} a_n \eta^n. \tag{39}$$

It follows from equations (32), (38), (19a) and (39) that

$$\Psi_1(\eta) \sim -\tfrac{2}{3} f_0(\infty)\eta \cot\left(\frac{2\pi}{3}\right) + A_1 + \tfrac{2}{3} f_0(\infty) \sum_{n=0}^{\infty} a_n \eta^n + \text{exp}, \quad \text{as } \eta \to \infty. \tag{40}$$

The above equations indicate that $\Psi_1(\eta)$ is singular at $X = 0$, i.e. when $\eta \to \infty$. To avoid this singularity, we set

$$a_1 = \cot\left(\frac{2\pi}{3}\right) \tag{41a}$$

and

$$a_n = 0, \quad \text{for } n = 2, 3, \ldots \tag{41b}$$

It follows from equations (39)–(41) and (19c) that

$$F(X, Y) = a_0 X^{1/3} + Y\cot\left(\frac{2\pi}{3}\right) \tag{42}$$

and

$$\Psi_1(\eta) \sim \tfrac{2}{3} f_0(\infty) a_0 + A_1 + \exp, \quad \text{as } \eta \to \infty. \tag{43}$$

To determine a_0, we assume that

$$\Psi_1(X, \infty) = 2A_1. \tag{44}$$

As we shall see in the next paragraph, this choice of $\Psi_1(X, \infty)$ would reduce the second-order outer problem for $\Psi_1(X, y)$ to the one in which the leading edge effect is absent.

Equating equation (43) to equation (44) gives

$$a_0 = \tfrac{3}{2}\frac{A_1}{f_0(\infty)}. \tag{45}$$

Substituting equation (45) into equation (42) yields

$$F(X, Y) = \tfrac{3}{2}\frac{A_1}{f_0(\infty)} X^{1/3} + Y\cot\left(\frac{2\pi}{3}\right). \tag{46}$$

It follows from equations (8c) and (46) that

$$x = X + \left[\tfrac{3}{2}\frac{A_1}{f_0(\infty)} X^{1/3} + Y\cot\left(\frac{2\pi}{3}\right)\right] Ra^{-1/3}. \tag{47}$$

At the leading edge where $x = y = 0$ and $X = X_0$, the above equation gives

$$X_0 = \left[-\tfrac{3}{2}\frac{A_1}{f_0(\infty)}\right]^{3/2} Ra^{-1/2} \tag{48}$$

where A_1 is given by equation (38). The value of X_0 is the distance between the origin of the thermal boundary layer and the leading edge, which is shown in Fig. 1.

Second-order outer problem

The second-order outer problem is given by

$$\psi_{1XX} + \psi_{1yy} = 2F_X \psi_{0XX} + F_{XX}\psi_{0X} \tag{49}$$

with the boundary condition

$$\psi_1(X, 0) = 0, \quad X < 0 \tag{50a}$$

and the matching condition from equation (50b) to give

$$\Psi_1(X, 0) = 2A_1, \quad X > 0. \tag{50b}$$

Letting

$$\tilde{\psi}_1 = \psi_1 - a_0 X^{1/3}\psi_{0X} \tag{51}$$

equations (49) and (50) in terms of $\tilde{\psi}_1$ become

$$\nabla^2 \tilde{\psi}_1 = 0 \tag{52}$$

$$\tilde{\psi}_1(X, 0) = 0, \quad X < 0 \tag{53a}$$

$$\tilde{\psi}_1(X, 0) = A_1, \quad X > 0. \tag{53b}$$

Equations (52) and (53) are the second-order outer problem for free convection of a Darcian fluid about a semi-infinite flat plate without the leading edge effect taken into consideration, which has been solved previously [19, 20]. It follows from equations (51) and (45) and refs. [19, 20] that

$$\psi_1 = A_1\left(1 - \frac{\Lambda}{\pi}\right) + \tfrac{3}{2}\frac{A_1}{f_0(\infty)} X^{1/3}\psi_{0X} \tag{54}$$

which gives

$$\psi_1(X, 0) = 2A_1 + A_1\left[\tfrac{1}{3}\cot\left(\frac{2\pi}{3}\right) - \frac{1}{\pi}\right] y/X + \ldots \tag{55}$$

Note that the second term on the right-hand side of equation (54) represents the leading edge effect for the second-order outer solution.

The third-order inner problem

The third-order inner problem is given by

$$\Psi_{2YY} - \Theta_{2Y} + \Psi_{0XX} = -F_Y^2\Psi_{0XX} + F_X F_Y(\Theta_0 - 2\Psi_{0XY}) - F_Y(\Theta_1 - 2\Psi_{1XY}) \tag{56}$$

and

$$\begin{aligned}\Theta_{2YY} &- (\Psi_{0Y}\Theta_{2X} - \Psi_{0X}\Theta_{2Y}) - (\Psi_{2Y}\Theta_{0X} - \Psi_{2X}\Theta_{0Y}) \\ &- (\Psi_{1Y}\Theta_{1X} - \Psi_{1X}\Theta_{1Y}) + \Theta_{0XX} \\ &= F_Y[2\Theta_{1XY} - 2F_X\Theta_{0XY} - F_Y\Theta_{0XX}] + F_Y(\Psi_{1X}\Theta_{0Y} \\ &- \Psi_{1Y}\Theta_{0X}) + F_X[\Psi_{0X}\Theta_{1Y} - \Psi_{0Y}\Theta_{1X}] \\ &+ F_X^2[\Psi_{0Y}\Theta_{0X} - \Psi_{0X}\Theta_{0Y}]\end{aligned} \tag{57}$$

subject to boundary conditions

$$\Psi_{2X}(X, 0) = 0, \quad \Theta_{2Y}(X, 0) = 0 \tag{58a, b}$$

and matching conditions

$$\begin{aligned}&\Psi_{2Y}(X, \infty) - F_Y(X, \infty)\Psi_{1X}(X, \infty) \\ &+ F_X(X, \infty)F_Y(X, \infty)\Psi_{0X}(X, \infty) = \psi_{1y}(X, 0)\end{aligned} \tag{59a}$$

$$\Theta_2(X, \infty) = 0. \tag{59b}$$

It can be shown that equations (56)–(59) admit a similarity solution of the form

$$\Psi_2(X, Y) = X^{-2/3} f_2(\eta) + \tfrac{1}{2}F^2\Psi_{0XX} + Ff_{1X} \tag{60}$$

$$\Theta_2(X, Y) = X^{-1} g_2(\eta) + \tfrac{1}{2}F^2\Theta_{0XX} + F\frac{\partial}{\partial X}(X^{-1/3} g_1). \tag{61}$$

Table 1. Some numerical results

$g_0(0)$	$f_0(\infty)$	$f_1'(0)$	$g_1(0)$	A_1	$f_2'(0)$	$g_2(0)$	a	b	c
1.2961	1.4818	0.1887†	−0.3816†	−0.8001	0.3431†	0.08862†	−0.2699	−0.2944	0.06837

† These values differ slightly from those obtained by Joshi and Gebhart [20].

Note that the first term on the right-hand side of equations (60) and (61) satisfy the left-hand side of equations (56) and (57), and that $f_2(\eta)$ and $g_2(\eta)$ are determined from

$$f_2''' = g_2' + \tfrac{2}{9} f_0 - \tfrac{1}{9}\eta^2 f_0'' \quad (62)$$

and

$$g_2'' + \tfrac{2}{3} f_0 g_2' + f_0' g_2 = \tfrac{1}{3} g_0 f_2' + \tfrac{2}{3} f_2 g_0' - \tfrac{1}{3} g_1 f_1' + \tfrac{2}{9} g_0 - \tfrac{2}{9}\eta g_0' - \tfrac{1}{9}\eta^2 g_0'' \quad (63)$$

subject to boundary conditions

$$f_2(0) = g_2'(0) = 0 \quad (64a, b)$$

$$g_2(\infty) = 0 \quad \text{and} \quad f_2'(\eta) = \tfrac{2}{9} f_0(\infty)\eta - \frac{A_1}{\pi}, \quad \text{as } \eta \to \infty \quad (65a, b)$$

where A_1 is determined from equation (38). Note that equations (62)–(65) have been solved by Joshi and Gebhart [20].

Eigenvalues and eigenfunctions

As shown by Joshi and Gebhart [20] the first eigenvalue of the problem is $\alpha_1 = 3/2$ and the corresponding eigenfunctions are

$$\Psi_{3/2}(X, Y) = \frac{C_1}{3} X^{-1/3}(2f_0 - \eta f_0') \quad (66a)$$

and

$$\Theta_{3/2}(X, Y) = \frac{C_1 X^{-2/3}}{3}(g_0 - \eta g_0') \quad (66b)$$

with $C_1 = 0$. Therefore, the asymptotic series given by equations (7a) and (7b) are valid to $O(\varepsilon^4)$ and $O(\varepsilon^3)$, respectively.

RESULTS AND DISCUSSION

The fourth-order Runge–Kutta method was used for the numerical solution of the first-, second-, and third-order inner problems given by equations (20)–(23), (34)–(37), and (62)–(65), respectively. Some of the results of the numerical integration are tabulated in Table 1 for future reference.

From equations (7a), (19a), (32) and (60), it can be shown that the vertical velocity component in the thermal boundary layer is

$$\frac{u}{x\varepsilon_x} = f_0'(\eta) + \varepsilon_x\{f_1'(\eta) + L(\eta)[f_0'(\eta) - \eta f_0''(\eta)]\} + \varepsilon_x^2\left\{f_2'(\eta) + L^2(\eta)\left[\frac{\eta^2}{2} f_0'''(\eta) + \eta f_0''(\eta) - f_0'(\eta)\right] - L(\eta)[f_1'(\eta) + \eta f_1''(\eta)]\right\} + O(\varepsilon_x^3) \quad (67)$$

where

$$L(\eta) = \tfrac{1}{3}\eta \cot\left(\frac{2\pi}{3}\right) + \tfrac{1}{2}\frac{A_1}{f_0(\infty)}$$

and

$$\varepsilon_x = Ra_x^{-1/3}$$

with

$$Ra_x = g\beta K q_w \hat{x}^2/\alpha\nu k.$$

It is pertinent to note that the terms associated with $L(\eta)$ in equation (67) represent the leading edge effect. Without these terms, equation (67) reduces to the solution obtained by Joshi and Gebhart [20]. Equation (67) with and without the leading edge effect is computed for $Ra_x = 10^2$ and 10^3, and plotted in Figs. 2(a) and (b), respectively. The vertical velocity profiles

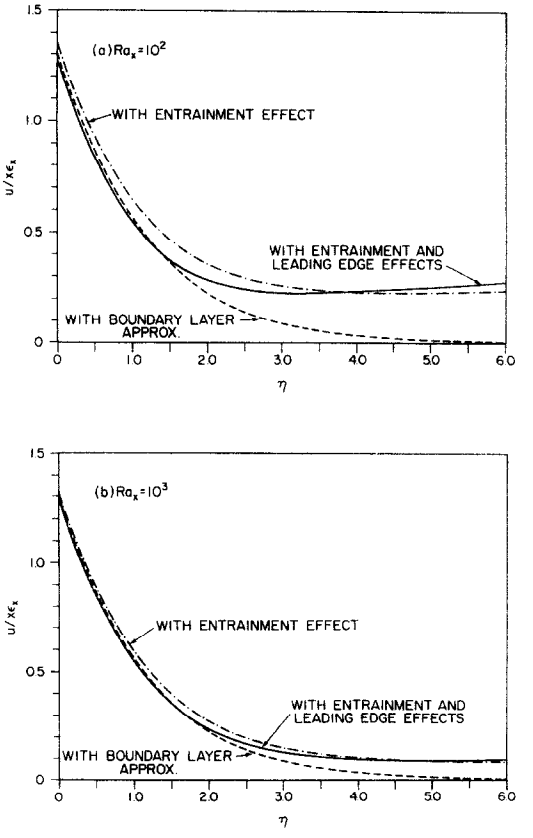

FIG. 2. Dimensionless vertical velocity profiles at: (a) $Ra_x = 10^2$; (b) $Ra_x = 10^3$.

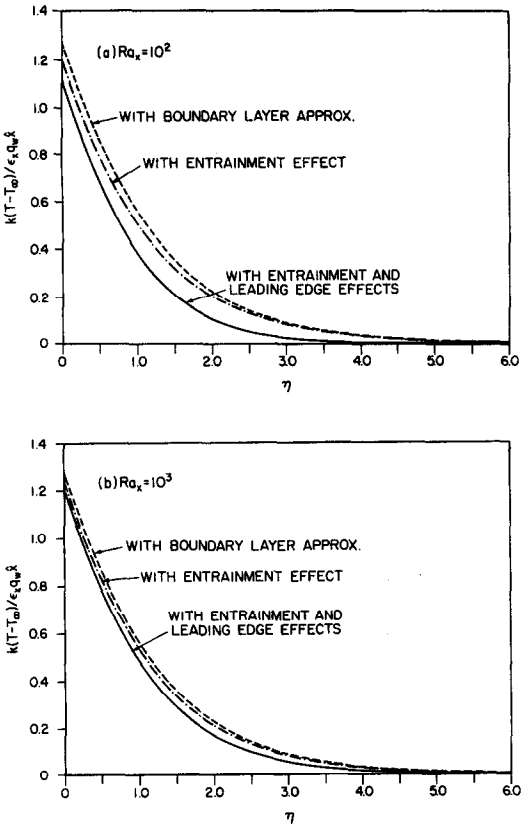

FIG. 3. Dimensionless temperature profiles at: (a) $Ra_x = 10^2$; (b) $Ra_x = 10^3$.

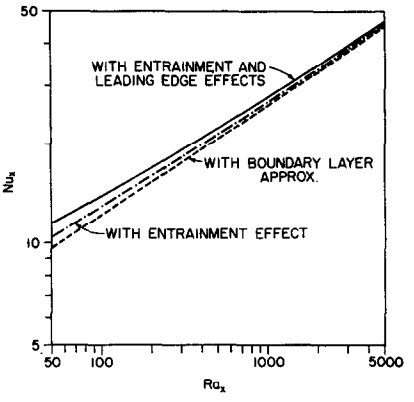

FIG. 4. Leading edge and entrainment effects on the local Nusselt number.

based on the boundary layer approximation (i.e. the first term of equation (63)) are also presented as dashed lines in these figures for comparison purposes. The leading edge effect is shown to increase the vertical velocity near the outer edge of the thermal boundary layer, but decreases slightly the vertical velocity adjacent to the plate. In comparison of Figs. 2(a) and (b), it is shown that the boundary layer entrainment and leading edge effects decrease as the value of Ra_x is increased.

The dimensionless temperature distribution as obtained from equations (7b), (19b), (33) and (61) is

$$\frac{(T-T_\infty)}{x\varepsilon_x q_w l/k} = g_0(\eta)+\varepsilon_x\{g_1(\eta)+L(\eta)[g_0(\eta)-\eta g_0'(\eta)]\}$$
$$+\varepsilon_x^2\left\{g_2(\eta)-L(\eta)[g_1(\eta)+\eta g_0'(\eta)]+L^2(\eta)\right.$$
$$\left.\times\left[-g_0(\eta)+\eta g_0'(\eta)+\frac{\eta^2}{2}g_0''(\eta)\right]\right\}+O(\varepsilon_x^3). \quad (68)$$

Equation (68) is plotted for $Ra_x = 10^2$ and 10^3 in Figs. 3(a) and (b), respectively. It is shown that both the leading edge effect and the boundary layer entrainment effect result in negative corrections to the temperature distribution based on the boundary layer theory. A comparison of Figs. 3(a) and (b) indicates that these effects are more pronounced as the local Rayleigh number is decreased.

It follows from equation (68) that the surface temperature of the plate is given by

$$\frac{(T_w-T_\infty)}{x\varepsilon_x q_w l/k} = g_0(0)[1+(a+b)\varepsilon_x$$
$$-(a^2+ab-c)\varepsilon_x^2+O(\varepsilon_x^3)] \quad (69)$$

with

$$a = L(0) = \tfrac{1}{2}\frac{A_1}{f_0(\infty)}, \quad b = g_1(0)/g_0(0)$$

and

$$c = g_2(0)/g_0(0)$$

where the terms associated with a denote the leading edge effect. The computed values of a, b and c are listed in Table 1.

With the aid of equation (69), the local Nusselt number is given by

$$Nu_x = \frac{q_w\hat{x}}{k(T-T_\infty)_w} = \frac{1}{\varepsilon_x g_0(\eta)}[1-(a+b)\varepsilon_x$$
$$+(2a^2+3ab+b^2-c)\varepsilon_x^2+O(\varepsilon_x^3)] \quad (70)$$

which is presented as a function of the local Rayleigh number in Fig. 4. From this figure, it is shown that both the leading edge and the boundary layer entrainment effects increase the surface heat flux as compared to that predicted based on the boundary layer approximation. These effects contribute almost equally to the increase in the heat transfer rate. At $Ra_x < 100$, the combined effects enhance the heat transfer rate by more than 10% over those predicted by the boundary layer approximation. Their effects decrease as the value of Ra_x is increased.

The local Nusselt number ratio is given by

$$\frac{Nu_x}{(Nu_x)_{B.L.}} = 1-(a+b)\varepsilon_x$$
$$+(2a^2+3ab+b^2-c^2)\varepsilon_x^2+O(\varepsilon_x^3) \quad (71)$$

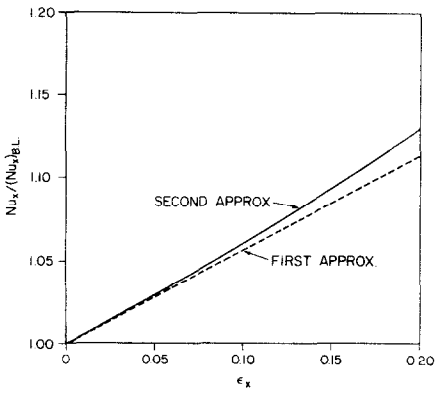

FIG. 5. First- and second-order approximations for the normalized local Nusselt number.

where $(Nu_x)_{B.L.} = 1/\varepsilon_x g_0(0)$ is the local Nusselt number based on the boundary layer approximation. The first and the second approximations given by equation (71) are plotted respectively as dashed lines and a solid line in Fig. 5 as a function of ε_x. It is shown that the local Nusselt number ratio increases from unity as the value of ε_x is increased from zero.

CONCLUDING REMARKS

The idea of deformed coordinates used in this paper is deduced from experimental observations that the boundary layer begins not at the leading edge of the plate, but at a distance ahead of the leading edge. With the aid of a deformed longitudinal coordinate, it is possible to shift the singularities in the inner solution of the boundary layer equations to their true position, and to determine more precisely the origin of the boundary layer relative to the leading edge. The structure of the boundary layer interaction with the outer flow is preserved under the coordinate transformation.

It is shown that the leading edge effect in the present problem manifests itself as inhomogeneous terms in the second- and third-order problems. The leading edge and entrainment effects are found to increase the heat transfer rate by approximately the same amount. These effects increase as the Rayleigh number is decreased.

REFERENCES

1. K. Brodowicz, An analysis of laminar free convection around isothermal vertical plate, *Int. J. Heat Mass Transfer* **11**, 201–209 (1968).
2. M. G. Scherberg, Natural convection near and above thermal leading edges on vertical walls, *Int. J. Heat Mass Transfer* **5**, 1001–1010 (1962).
3. C. A. Hieber, Natural convection around a semi-infinite vertical plate: higher-order effects, *Int. J. Heat Mass Transfer* **17**, 785–791 (1974).
4. O. G. Martynenko, A. A. Berezovsky and Yu. A. Sokovishin, Laminar free convection from a vertical plate, *Int. J. Heat Mass Transfer* **27**, 869 881 (1984).
5. P. Cheng and W. J. Minkowycz, Free convection about a vertical flat plate embedded in a porous medium with application to heat transfer from a dike, *J.G.R.* **82**, 2040–2044 (1977).
6. P. Cheng, Constant surface heat flux solutions for porous layer flows, *Lett. Heat Mass Transfer* **4**, 119–127 (1977).
7. P. Cheng, Heat transfer in geothermal systems, *Adv. Heat Transfer* **14**, 1–105 (1978).
8. P. Cheng, Heat transfer in porous media : external flows. In *Natural Convection : Fundamentals and Applications* (Edited by S. Kakac, W. Aung and R. Viskanta), pp. 475–513. Martinus Nijhoff, The Hague, The Netherlands (1985).
9. G. H. Evans and O. A. Plumb, Natural convection from a vertical isothermal surface imbedded in a saturated porous medium, AIAA–ASME Thermophysics and Heat Transfer Conference, Paper No. 78-HT-55, Palo Alto, California (1978).
10. P. Cheng, C. L. Ali and A. K. Verma, An experimental study of non-Darcian effects in free convection in a saturated porous medium, *Lett. Heat Mass Transfer* **8**, 261–266 (1981).
11. P. Cheng and C. L. Ali, An experimental investigation of free convection about an inclined surface in a porous medium, 20th National Heat Transfer Conference, Paper No. 81-HT-85 (August 1981).
12. J. S. Huenefeld and O. A. Plumb, A study of non-Darcy natural convection from a vertical heated surface in a saturated porous medium, 20th National Heat Transfer Conference, Paper No. 81-HT-45 (August 1981).
13. O. A. Plumb and J. C. Huenefeld, Non-Darcy natural convection from heated surfaces in saturated porous media, *Int. J. Heat Mass Transfer* **24**, 765–768 (1981).
14. A. Bejan and D. Poulikakos, The non-Darcy regime for vertical boundary layer natural convection in a porous medium, *Int. J. Heat Mass Transfer* **27**, 717–722 (1984).
15. J. T. Hong, C. L. Tien and M. Kaviany, Non-Darcian effects on vertical-plate natural convection in porous media with high porosities, *Int. J. Heat Mass Transfer* **28**, 2149–2157 (1985).
16. J. T. Hong, Y. Yamada and C. L. Tien, Effects of non-Darcian and non-uniform porosity on vertical plate natural convection in porous media, *J. Heat Transfer* **109**, 357–362 (1987).
17. O. A. Plumb, The effect of thermal dispersion on heat transfer in packed bed boundary layers, *Proc. ASME–JSME Thermal Engineering Conference*, Vol. 2, pp. 17–22 (1983).
18. J. T. Hong and C. L. Tien, Analysis of thermal dispersion effect on vertical-plate natural convection in porous media, *Int. J. Heat Mass Transfer* **30**, 143–150 (1987).
19. P. Cheng and C. T. Hsu, Higher-order approximations for Darcian free convective flow about a semi-infinite vertical flat plate, *J. Heat Transfer* **106**, 143–151 (1984).
20. Y. Joshi and B. Gebhart, Vertical natural convection flows in porous media : calculations of improved accuracy, *Int. J. Heat Mass Transfer* **27**, 69–75 (1984).

EFFETS DU BORD D'ATTAQUE SUR LA CONVECTION NATURELLE D'UN FLUIDE DARCIEN AUTOUR D'UNE PLAQUE SEMI-INFINIE VERTICALE AVEC FLUX DE CHALEUR UNIFORME

Résumé—La méthode des développements asymptotiques, avec une coordonnée longitudinale déformée, est appliquée à l'étude de l'effet du bord d'attaque sur la convection naturelle autour d'une surface verticale, semi-infinie, noyée dans un milieu poreux, avec flux de chaleur uniforme. Cet effet se manifeste par des termes non homogènes dans les problèmes de second et troisième ordre. Des solutions de similitude pour l'écoulement de convection naturelle dans un milieu poreux sont obtenues jusqu'à l'approximation du troisième ordre. On montre que l'effet du bord d'attaque augmente la vitesse verticale près de la frontière extérieure de la couche limite, avec un accroissement correspondant du flux thermique à la surface. Les effets de bord d'attaque et d'entrainement augmentent le transfert de chaleur à peu près également. A $Ra_x = 100$, les effets combinés accroissent le transfert de chaleur de plus de 10% par rapport au cas basé sur l'approximation de couche limite. Ces effets augmentent quand le nombre de Rayleigh décroît.

EINFLUSS DER ANSTRÖMKANTE AUF DIE FREIE KONVEKTION EINES DARCY-FLUIDS AN EINER HALBUNENDLICHEN, VERTIKALEN, GLEICHFÖRMIG BEHEIZTEN PLATTE

Zusammenfassung—Das Verfahren der angepaßten asymptotischen Reihenentwicklung wurde in Verbindung mit einer verformten Längskoordinate angewendet, um den Einfluß der Anströmkante auf die freie Konvektion an einer halbunendlichen, vertikalen, gleichförmig beheizten Platte in einem porösen Medium zu untersuchen. Der Einfluß der Anströmkante geht in Form inhomogener Terme in die Gleichungen zweiter und dritter Ordnung ein. Ähnlichkeitslösungen für die Konvektionsströmung im porösen Medium werden bis zur Näherung 3. Grades angegeben. Es zeigt sich, daß der Einfluß der Anströmkante die vertikale Geschwindigkeit nahe des äußeren Randes der thermischen Grenzschicht erhöht und zu einer entsprechenden Erhöhung der Wärmestromdichte an der Oberfläche führt. Es wird gezeigt, daß die Einflüsse von Anströmkante und Entrainment den Wärmeübergang etwa gleich stark verbessern. Bei $Ra_x = 100$ erhöhen die gekoppelten Effekte den Wärmeübergang um mehr als 10%—verglichen mit den aus den Grenzschichtvereinfachungen errechneten Werten. Die Einflüsse verstärken sich mit sinkender Rayleigh-Zahl.

ВЛИЯНИЕ ПЕРЕДНЕЙ КРОМКИ РАВНОМЕРНО НАГРЕВАЕМОЙ ПОЛУОГРАНИЧЕННОЙ ВЕРТИКАЛЬНОЙ ПЛАСТИНЫ НА СВОБОДНУЮ КОНВЕКЦИЮ ЖИДКОСТИ, ПОДЧИНЯЮЩУЮСЯ ЗАКОНУ ДАРСИ

Аннотация—Методом сращиваемых асимптотических разложений с использованием деформированной продольной координаты исследовалось влияние передней кромки на свободную конвекцию вокруг равномерно нагреваемой полуограниченной вертикальной пластины, помещенной в пористую среду. В связи с эффектом передней кромки в разложениях второго и третьего порядка появляются неоднородные члены. Для свободноконвективного течения в пористой среде для разложений с точностью 3-го порядка получены автомодельные решения. Показано, что из-за эффекта передней кромки скорость направленного вертикально вверх потока у внешнего края теплового пограничного слоя увеличивается, в результате чего возрастает и тепловой поток на поверхности пластины. Показано также, что как эффект передней кромки, так и эффект уноса почти одинаково влияют на увеличение интенсивности теплопереноса. При $Ra_x = 100$ оба эти эффекта усиливают интенсивность теплопереноса более чем на 10% по сравнению с величиной, рассчитываемой на основе приближения пограничного слоя. Влияние эффектов усиливается с уменьшением числа Рэлея.